

Marrubium vulgare Leaf Extract-Assisted Green Synthesis of Silver Nanoparticles: Optimization, Characterization and In Vitro Exploration of Their Antimicrobial, Antioxidant and Anti-Inflammatory Potential

Sarra Abbad^{1*}, Nadia Aissaoui², Fatima Zahra Gana^{1,3}

Sarra Abbad^{1*}, Nadia Aissaoui²,
Fatima Zahra Gana^{1,3}

¹Department of Pharmacy, Faculty of Medicine,
Abou Bekr Belkaid University, Tlemcen 13000,
ALGERIA.

²Laboratory of Sustainable Management of
Natural Resources in Arid and Semi-arid Areas,
University Center of Naama, Naama 45000,
ALGERIA.

³Laboratory of Analytical Chemistry and
Electrochemistry, Abou Bekr Belkaid University,
Tlemcen 13000, ALGERIA.

Correspondence

Sarra Abbad

Department of Pharmacy, Faculty of
Medicine, Abou Bekr Belkaid University,
Tlemcen 13000, ALGERIA.

E-mail: sarra.abbad@univ-tlemcen.dz

History

- Submission Date: 16-11-2024;
- Review completed: 20-12-2024;
- Accepted Date: 06-01-2025.

DOI : 10.5530/pj.2025.17.2

Article Available online

<http://www.phcogj.com/v17/i1>

Copyright

© 2025 Phcogj.Com. This is an open-
access article distributed under the terms
of the Creative Commons Attribution 4.0
International license.

ABSTRACT

Background: Biogenic metal nanoparticles are gaining popularity due to their remarkable biomedical properties, which provide hope in the fight against various diseases. **Objective:** This research produced silver nanoparticles (AgNPs) from an aqueous extract of *Marrubium vulgare* leaves by a simple, one-step, bottom-up green route. For the first time in the literature, the antimicrobial, antioxidant, and anti-inflammatory potentials of AgNPs obtained using leaves of *Marrubium vulgare* are investigated. **Methods and results:** The optimal conditions for biosynthesis were 80 °C reaction temperature, 60 min incubation time, 2 mM AgNO₃, and 100 µL extract volume. The FTIR results indicated that the distinct functional groups found in *M. vulgare* extract were also present in AgNPs, confirming their critical role in silver bioreduction and AgNP capping. The biosynthesized AgNPs were crystalline, with face-centered cubic geometry, according to XRD analysis. DLS analysis asserted that the constructed AgNP's average size was 34.58 nm, whereas SEM/TEM revealed their spherical morphology. The AgNPs produced through biosynthesis inhibited microbial proliferation in a dose-dependent manner. They exhibited bactericidal attributes against both Gram-negative and Gram-positive bacteria, with MIC values ranging from 0.041 to 5.312 µg/mL and MBCs from 0.083 to 5.312 µg/mL. Furthermore, the AgNPs exhibited fungicidal activity against three *Candida albicans* strains, with MIC and MFC respective values recorded at 2.656 and 2.656-5.312 µg/mL. Additionally, the biosynthesized AgNPs demonstrated significant antioxidant potency compared to ascorbic acid and the extract. Their potent in vitro anti-inflammatory effect, attributed to the inhibition of BSA denaturation, was directly proportional to the AgNP concentration, with a maximum inhibition of 86.14% observed at 200 µg/mL. **Conclusion:** Therefore, the findings suggest that AgNPs have promising applications in combating the growing threat of antimicrobial resistance and might be utilized as potent antioxidant and anti-inflammatory agents.

Keywords: Silver nanoparticles, Green synthesis, *Marrubium vulgare*, Characterization, Biological activities.

INTRODUCTION

Nanotechnology, as a swiftly advancing discipline, is enabling the development of biocompatible nanomaterials with the capacity to transform the diagnosis and management of various diseases. The growing interest in using these nanomaterials in medicine stems from their large spectrum of benefits over conventional formulations. Nanoparticles, generally measuring between 1 and 100 nm, distinguished by their high surface-to-volume ratio, have distinct physical and chemical properties that differ from the bulk material¹. Among these nanomaterials, silver nanoparticles (AgNPs) are the most extensively studied and fastest-growing nanotechnology-based products². AgNPs, as noble metal nanoparticles, are highly desirable due to their high stability, ease of preparation, and exceptional optical, electrical, catalytic, and biological properties^{3,4}. The distinct characteristics of AgNPs have been applied across multiple fields, including medicine, pharmaceuticals, cosmetics, food science, the textile industry, electronics, biosensors and bioimaging, water waste treatment, renewable energies,

and environmental remediation^{5,6}. Of the many beneficial biological effects attributed to AgNPs, the most crucial and thoroughly studied aspect of AgNPs is their antimicrobial activity against diverse microorganisms⁷.

Multidrug-resistant pathogenic microorganisms such as bacteria, fungi, viruses, and parasites have emerged and spread globally in recent decades⁸. However, while thoughts about the COVID-19 pandemic have drawn all our attention, we should not overlook that resistance to antimicrobial agents is predicted to affect 10 million cases annually by 2050⁹. This current crisis of antimicrobial resistance, also referred to as the silent pandemic, has worsened due to the heightened utilization of antimicrobials in treating COVID-19 patients¹⁰. One of the most critical global health concerns is antimicrobial resistance, which raises the escalating risk of reaching a therapeutic standstill. According to the World Health Organization (WHO), inappropriate and excessive antimicrobial use are the primary causes of this phenomenon's dramatic increase¹¹. Worryingly, the lack of newly developed antimicrobial drugs, combined with the rapid evolution of antimicrobial

Cite this article: Abbad S, Aissaoui N, Gana FZ. *Marrubium vulgare* Leaf Extract-Assisted Green Synthesis of Silver Nanoparticles: Optimization, Characterization and In Vitro Exploration of Their Antimicrobial, Antioxidant and Anti-Inflammatory Potential. Pharmacogn J. 2025;17(1): 7-21.

resistance, will soon usher in a post-antibiotic era¹². Hence, there is a high demand for alternative strategies to combat antimicrobial resistance and overcome conventional antimicrobial therapy. Nanotechnology-based advancements have introduced a novel class of potential antimicrobial candidates, able to combat drug resistance in a range of pathogenic microorganisms. Recent advances in nanotechnology have enabled the creation of metallic nanoparticles that can act as antimicrobial carriers or antimicrobials themselves, thereby providing a new line of defense against resistant microorganisms¹³.

Besides, several research studies have shown that silver nanoparticles possess antioxidant potential and can mitigate oxidative stress through eliminating free radicals. The onset and progression of numerous diseases, including cancer, diabetes, neurodegenerative disorders, and cardiovascular diseases, are linked to oxidative stress resulting from imbalances among reactive oxygen species (ROS) synthesis and the biological system's capacity to combat them¹⁴. AgNPs demonstrating antioxidant activity could be vital in the anticipation of such dysfunctions. Recently, increasing attention has also been given to utilizing AgNPs for the treatment of inflammatory conditions. The human body responds to potentially harmful stimuli such as injury or infection through a defensive complex inflammation process. However, persistent inflammation and failure to restore tissue homeostasis can contribute to the development of chronic inflammatory diseases. Inflammation is generally managed by a vast array of pharmaceutical agents. Despite the availability of a therapeutic arsenal, the prolonged use of anti-inflammatory drugs has been associated with side effects, which have hampered the effectiveness of these drugs, deepening the need for new anti-inflammatory drug candidates. As a result, many studies have explored the therapeutic efficacy of AgNPs as anti-inflammatory agents with fewer side effects.

AgNPs are typically produced through traditional chemical and physical techniques, including chemical reduction, laser ablation, hydrothermal method, electrochemical reduction, chemical vapor deposition, photochemical reduction, microwave irradiation, and the sol-gel process^{6,15}. Nonetheless, most of these methods have drawbacks, including elevated operational costs, excessive energy consumption, the use of hazardous chemicals, and the production of byproducts that pollute the environment^{16,17}. As a result of growing concern about environmental risks, interest in green nanoparticles synthesis has increased. In this regard, a plethora of biological sources, involving bacteria, fungi, yeasts, algae, and plants, have been used to facilitate AgNP synthesis¹⁸. Employing plant extracts for the biogenic synthesis of AgNPs presents benefits compared to alternative biological approaches because it eliminates the necessity for complicated cell culture maintenance and extensive extraction and purification processes¹⁹.

Plant-mediated synthesis of AgNPs gained popularity nowadays due to its quick, environmentally friendly, cost-effective, and easily scaleable protocol^{20,21}. In this plant-based method, phytochemicals found in extracts such as amino acids, proteins, flavonoids, enzymes, phenolic compounds, tannins, and terpenoids reduce silver ions and stabilize the formed AgNPs²². To date, different plant parts have been used to synthesize AgNPs, including *Eugenia roxburghii* leaves²³, *Astragalus tribuloides* Delile roots²⁴, *Syzygium cumini* fruits²², *Persea Americana* seeds²⁵, *Annona senegalensis* stem bark²⁶, and *Alpinia galangal* rhizome²⁷.

Marrubium vulgare L., a perennial herbaceous medicinal plant from the Lamiaceae family, is originated from North Africa, Europe, and Western Asia²⁸. *M. vulgare* is also called white horehound in Europe, "Marriout" in Algeria²⁹, "Marrubia" in Tunisia³⁰, and "Merritw" in Morocco³¹. In Algerian folk medicine, *M. vulgare* is used to cure various ailments, particularly gastrointestinal disorders, bronchitis, coughs, colds, hypertension, and diabetes^{29,32}. A variety of in vivo and in vitro research indicated that *M. vulgare* has antimicrobial, antioxidant,

anti-inflammatory, analgesic, hypolipidemic, antiedematogenic, hypoglycemic, and anticancer properties^{33,34}. The European Medicines Agency has published a monograph on *M. vulgare*'s therapeutic properties, including traditional indications, non-clinical and clinical data, and pharmacovigilance³⁵. Previous phytochemical analyses of this plant highlighted bioavailability of phenolic acids, flavonoids, phenylpropanoid esters, tannins, alkaloids, diterpenoids, and a moderate amount of essential oils, among other phytochemicals^{36,37}. Given the reducing abilities of some of these molecules, we present the first attempt to develop a simple and sustainable method for synthesizing AgNPs from aqueous *M. vulgare* leaf extract. Although Lupuliasa et al. have previously reported the production of AgNPs employing a hydroalcoholic extract of the aerial part of *M. vulgare* and the evaluation of the biocompatibility of AgNPs with human gingival fibroblasts (HGFs)³⁸, this is the first report to quantify the anti-inflammatory, antioxidant, and antimicrobial potency of AgNPs synthesized using *M. vulgare* aqueous leaf extract. The key operational parameters influencing the reaction rate of AgNP synthesis and the size distribution, such as temperature, silver nitrate concentration, extract volume, and reaction time, were thoroughly examined. Characterization of the biosynthesized AgNPs was performed using multiple analytical procedures, enumerating: the DLS (dynamic light scattering), transmission electron microscopy (TEM), the XRD (X-ray diffraction), UV-Vis spectroscopy, scanning electron microscopy (SEM) coupled with energy dispersive X-ray (EDX) analysis, along with Fourier transform infrared (FTIR) spectroscopy. Furthermore, the antibacterial and antifungal activities of as-prepared AgNPs were tested against various bacterial and fungal strains. The antioxidant efficacy of the phytosynthesized AgNPs was assessed by DPPH and ABTS assays. Finally, the anti-inflammatory activity of AgNPs was scrutinized using the protein denaturation method.

MATERIALS AND METHODS

Materials

Silver nitrate (AgNO_3), 1,1-diphenyl-2-picrylhydrazyl (DPPH) were sourced from VWR Chemicals. Folin Ciocalteu, gallic acid, 2,2'-Azino-bis(3-ethylbenzthiazoline-6-sulfonic acid) (ABTS), bovine serum albumin (BSA), diclofenac sodium, Levofloxacin (LEV) and Amphotericin B (AmpB) were acquired from Sigma-Aldrich (Darmstadt, Germany). Muller-Hinton Agar and Muller-Hinton broth were purchased from Conda Pronadisa (Madrid, Spain). Sabouraud Dextrose Agar (SDA) was procured from Liofilchem, Italy. Ultra-pure water (Milli-Q, resistivity 18.2 M Ω -cm at 25 °C) was employed in all experiments. Analytical-grade ethanol was utilized.

Plant sample and preparation of the aqueous extract

The dried leaves of *M. vulgare* were obtained from a local market in Tlemcen, Algeria, and identified by a botanical expert from the Department of Pharmacy, Tlemcen University. These components were meticulously rinsed using distilled water to cleanse residual dust and unwanted particles, shade-dried for two weeks, the material was then finely ground using a milling machine (IKA-Werke, GMBH and Co., Germany). To prepare the aqueous extract, 10 g of leaf powder was added to 100 mL of Milli-Q water in a 250 mL round-bottom flask. The extraction process was performed at 100 °C under reflux for one hour. After cooling, the mix was passed by a Whatman filter paper, and the collected filtrate was stored at 4 °C for future use.

Determination of total phenolic content (TPC)

The determination of total phenolic compounds in the aqueous extract was performed using the Folin-Ciocalteu protocol, as detailed according to C. Singh et al., with small tweaks made to the original protocol³⁹. Briefly, 1 mL of distilled water, 100 μL of the aqueous

extract (1 mg/mL), and 200 μ L of 2 M Folin-Ciocalteu reagent were successively placed in a tube and mixed using a vortex. After 15 min of incubation at room temperature, 2 mL of 7 % sodium carbonate solution was incorporated to neutralize the reaction, followed by 0.7 mL of distilled water to increase the volume of the reaction mixture to 4 mL. Subsequently, the tube was shaken and kept in the shade for 2 h at ambient conditions. Absorbance was then recorded at 755 nm, using a blank as a reference, with a UV-visible spectrophotometer (Jenway 6850, Cole-Parmer). The TPC of the extract was evaluated by a calibration curve with standard gallic acid (0–500 μ g/mL). Values were reported in milligrams of gallic acid equivalents (GAE) per gram of dry extract, and each experiment was repeated three times.

Synthesis of silver nanoparticles (AgNPs)

In a clean 25 mL Erlenmeyer flask, a certain volume from the aqueous extract was homogenized with 9 mL of freshly prepared AgNO₃ solution at the required concentration for rapid biosynthesis of AgNPs. The solution was heated at 80 °C for the desired reaction time while being continuously stirred in the dark. The formation of AgNPs was indicated by a clear color transition in the reaction mix from pale yellow to colloidal brown. Following that, the colloidal mixture underwent centrifugation at 13,000 rpm for 30 minutes in a refrigerated centrifuge (Sigma 2-16PK, Germany) to separate AgNPs. The pellet was further purified from silver ions and unbound phytochemicals by repeated dispersion-centrifugation cycles, twice with MilliQ water and once with pure ethanol. The precipitated AgNPs were then placed in a hot air oven at 45 °C for 5 h to dry and then stored at 4 °C for further experiments.

Optimization of silver nanoparticle synthesis

The optimization process was carried out by investigating the effect of four operational parameters, including temperature, AgNO₃ concentration, aqueous extract volume, and reaction time, on AgNP formation, using the protocol of Assimudin et al.⁴⁰. To study how temperature affects the rate of synthesis, reaction mixtures with 100 μ L of aqueous extract and 1 mM AgNO₃ were incubated for 1 h at variable temperatures (20, 30, 40, 50, 60, 70, 80 °C). The effect of silver ions on the biosynthesis of AgNPs was determined by varying the AgNO₃ concentration from 0.25 to 4 mM while maintaining a constant amount of leaf extract (100 μ L). Several volumes (50, 75, 100, 200, 300, 400, 500, 600, and 700 μ L) of aqueous leaf extract were tested while keeping the AgNO₃ concentration constant at 2 mM. The influence of reaction time was investigated by maintaining the reaction mixtures at optimum conditions during incubation (100 μ L extract, 2 mM AgNO₃, 80 °C) for 5, 10, 20, 30, 40, 50, and 60 min.

Characterization of the synthesized silver nanoparticles

The optical properties of AgNPs synthesized from *M. vulgare* extract were determined using UV-visible spectroscopy. After the samples were diluted with ultrapure water, the UV-visible absorption spectra of the AgNPs were characterized by a double-beam spectrophotometer (Unicam UV500, Thermo Spectronic, Cambridge, United Kingdom) with a 1 cm path length quartz cuvette. To identify the functional groups in biomolecules attached to AgNPs, Fourier Transform Infrared Spectroscopy (FTIR) of the leaf extract and AgNPs was performed using attenuated total reflectance (ATR) mode (Agilent Technologies Cary 600 Series FTIR spectrometer). The FTIR analysis was conducted with spectra recorded between 600 and 4000 cm⁻¹.

A Rigaku Ultima IV X-ray diffractometer (Tokyo, Japan) was utilized to analyze the AgNPs, employing Cu-K α radiation across a 2 θ range of 20° to 90°. The settings included a voltage of 40 kV and a current of 40 mA. Moreover, dynamic light scattering (DLS) measurements of the AgNPs' average size and polydispersity index were conducted

at a temperature of 25.0 \pm 0.1 °C employing a Malvern Zetasizer Nano ZS instrument (Malvern, UK) with a scattering angle of 90°. The instrument fitting data directly measured the mean size of ten runs. The morphological nature of AgNPs was investigated using a scanning electron microscope (TM 1000, Hitachi, Chiyoda, Japan). The elemental composition measurements were performed using the same instrument, which was equipped with an EDX detector. The purified AgNPs were subjected to morphological analysis using transmission electron microscopy (TEM) on a JEM-2100 electron microscope (JEOL, Tokyo, Japan) with an accelerating voltage of 80 kV. A drop of the phyto-synthesized AgNPs was applied to a copper grid and left to dry at ambient temperature before analysis.

Evaluation of the antimicrobial activity of biosynthesized AgNPs

Microbial strains

The antimicrobial potential of AgNPs, AgNO₃, and the plant extract was screened against six Gram-positive bacteria (Methicillin-Susceptible *Staphylococcus aureus* (MSSA) ATCC 25923, Methicillin-Resistant *S. aureus* (MRSA) ATCC 43300, *Enterococcus faecalis* ATCC 49452, *Micrococcus luteus* ATCC 9341, *Bacillus cereus* ATCC 10876, *B. subtilis* ATCC 6633), three Gram-negative bacteria (*Pseudomonas aeruginosa* ATCC 27853, *Escherichia coli* ATCC 25912, *Klebsiella pneumoniae* ATCC 700603), and three yeasts (*Candida albicans* ATCC 10231, *Candida albicans* ATCC 26790, *Candida albicans* IPP444).

Agar well diffusion assay

The well diffusion method on agar was carried out as described by Nanda and Saravanan⁴¹. Using sterile swabs, the inoculum of each microorganism (10⁸ CFU/mL) was evenly distributed on Muller-Hinton Agar (MHA) for bacteria or Sabouraud Dextrose Agar (SDA) supplemented with glucose (2%) for yeasts. Agar plates were punctured with 5 mm diameter wells using sterile Pasteur pipette tips and loaded with increasing amounts (10, 25, 50, 75, and 100 μ L) of aqueous extract, AgNO₃ (50 μ g/mL), and AgNPs (50 μ g/mL). Incubation of the plates occurred for 24 h at 37 °C for bacteria and 28 °C for yeasts. After this period, the zones of inhibition (ZOI) were calculated. Afterward, the obtained zones of inhibition (ZOI) were measured. All assays were performed in triplicate, and the outcomes are expressed as mean \pm standard deviation (SD).

MIC, MBC and MFC determination

Minimum Inhibitory Concentrations (MICs) were assessed using the microbroth dilution method, as described by Arsene et al.⁴², with some modifications. Briefly, the wells of 96-well microplates were filled with 100 μ L of sterile MH broth or SD broth. The first wells received 100 μ L of either AgNPs (340 μ g/mL) or AgNO₃ (340 μ g/mL). After thoroughly mixing the contents, a series of 2-fold dilutions was executed by moving 100 μ L from the first wells to the subsequent wells, and so forth. The last 100 μ L of diluted compounds were discarded. Then, 100 μ L of each inoculum (\sim 5 \times 10⁵ CFU/mL for bacteria and \sim 5 \times 10⁴ CFU/mL for yeasts) was added in all wells. The microplates were sealed and incubated for 24 hours at 28 °C for yeasts and 37 °C for bacteria. The MIC was established as the most reduced concentration of the compound that successfully prevented visible growth of the target bacteria or yeast. The MIC values of the standard antibiotic Levofloxacin and the standard antifungal drug Amphotericin B were also determined. Each trial was performed in triplicate.

To ascertain the MBC (Minimum Bactericidal Concentration) and MFC (Minimum Fungicidal Concentration) respectively, the contents of the wells that demonstrated no growth in the MIC assessment were sub-cultured. For that, 100 μ L of culture from each well was spread

onto MHA or SDA plates and incubated at 37 °C for bacteria and at 28 °C for yeasts for 24 h. The most reduced concentration of compounds that eliminated 100% of the initial microbial population was noted as MBC or MFC. The MBC/MIC and MFC/MIC ratios were also calculated to assess the bactericidal/fungicidal effects (MBC/MIC \leq 4, MFC/MIC \leq 4) or bacteriostatic/fungistatic effects (MBC/MIC $>$ 4, MFC/MIC $>$ 4) of the evaluated AgNPs, AgNO₃, and standard drugs (LEV and Amp B)⁴³. MIC, MBC and MFC were obtained from three independent experiments.

Antioxidant activity of AgNPs

Assessment of DPPH free radical scavenging activity

The in vitro antioxidant properties of AgNPs and *M. vulgare* extract were tested using a DPPH radical scavenging assay. Briefly, 2 mL of different concentrations (10, 20, 40, 50, 60, 80, 100, 150 µg/mL) of *M. vulgare* extract and AgNPs were prepared and mixed with 2 mL of an ethanolic solution of DPPH (0.25 mM). The mixture underwent vortexing and was then incubated for 30 minutes in ambient conditions in the absence of light. Ascorbic acid acted as a standard antioxidant at comparable concentrations. Absorbance was noted at 517 nm to assess the reduction in DPPH concentrations using a UV-visible spectrophotometer (Jenway 6850, Cole-Parmer). DPPH (containing all reagents except the sample) was used as a control, while ethanol was used as a blank. The inhibition percentage, reflecting the capacity to scavenge DPPH, was computed based on the following formula:

$$\% \text{ of scavenging} = \frac{Ac - Ae}{Ac} \times 100$$

In this equation, Ac refers to the control absorbance, while Ae denotes the sample absorbance.

The assay was repeated in triplicate, with the results expressed as mean \pm standard deviation (SD). In addition, the IC₅₀ values (half maximal inhibitory concentration) of the tested compounds were calculated using linear regression analysis.

ABTS free radical scavenging assay

The ABTS assay was realized as previously outlined, with slight modifications⁴⁴. In summary, an ABTS solution (7 mM) was mixed with potassium persulfate (2.45 mM) in equal volumes to produce the ABTS \bullet radical, which was then incubated in the dark for 16 hours. The resulting mixture was then diluted to attain 0.700 \pm 0.02 of absorbance at 734 nm. This mixture was coupled with AgNPs and the extract at various concentrations ranging from (10 to 100 and 150 µg/mL) and incubated in the dark for 6 minutes. The corresponding absorbance was noted at 734 nm, with ascorbic acid serving as the standard. Antioxidant activity was determined using the standard formula described earlier for the DPPH assay.

Anti-inflammatory activity of AgNPs

An assessment of the anti-inflammatory effects of both biosynthesized AgNPs and *M. vulgare* extract was performed through the albumin denaturation inhibition assay. Diclofenac sodium was used as a reference drug. 1.0 mL of different concentrations of AgNPs, plant extract, and standard diclofenac sodium were admixed with 1 mL of 1% solution of bovine serum albumin then incubation was performed at 37 °C for 20 min. After incubation, denaturation of BSA was generated by keeping the reaction mixture for 30 min in a water bath at 70 °C. The mixtures were allowed to cool, and the absorbance of the specimens was noted at 660 nm. The protein denaturation activity was determined employing the following formula :

$$\% \text{ inhibition of protein denaturation} = \frac{Ac - Ae}{Ac} \times 100$$

Statistical analysis

Findings are represented as means \pm standard deviation (SD). Differences between samples were identified using one-way ANOVA with the post-hoc Tukey test, using SPSS 25.0 software; *p*-values $<$ 0.05 were considered significant.

RESULTS AND DISCUSSION

Total phenolic content

A significant number of studies on the plant-based green synthesis of AgNPs have shown that phytochemicals like phenolic compounds, alkaloids, terpenoids, saponins, proteins, polysaccharides, and other related biomolecules significantly influence AgNP formation. During the synthesis process, these biomolecules function as both stabilizing and reducing agents. The Folin-Ciocalteu method was employed to evaluate the TPC in an aqueous extract of *M. vulgare*. TPC was found to be 101 \pm 1.41 mg GAE/g dry extract. Several studies have shown that aqueous extracts of *M. vulgare* harvested in Algeria contain high levels of phenolic compounds, with the main classes being phenolic acids, phenylpropanoid esters, and flavonoids³⁶. Ghedadba et al. and Namoune et al.^{45,46} related that the aqueous extract of *M. vulgare* leaves contained 175.00 mg GAE/100 g dry matter and 48.62 \pm 1.73 mg GAE/g dry weight. These findings indicate that our extract exhibited the highest concentration of phenolic compounds. Variations in TPC between studies are primarily due to geographic origin, plant collection period, and extraction methods. Further investigation of the chemical composition of our extract may shed light on the biomolecules that can phytomediate AgNP synthesis.

Optical properties of synthesized AgNPs

The construction of AgNPs was monitored through the color shift of the reaction mix and by using UV-visible spectroscopy. In all experiments, adding plant extract to a colorless solution of silver nitrate caused the color to change to light yellow in a matter of minutes. The color increased with incubation time, and the reaction mixture turned brown, indicating the reduction of silver metal ions and the construction of nanoparticles (Figure 1a). Similar color changes have been observed by researchers investigating the green synthesis of AgNPs using plant extract. Al-Otibi et al. observed a color shift from light yellow to brown while synthesizing silver nanoparticles with an aqueous extract of grape seeds⁴⁷. The successful formation of AgNPs using *Carduus crispus* was also visually evidenced by a color shift from pale yellow to dark brown⁴⁸. According to Anbazhagan et al., AgNPs synthesized using microorganisms such as yeast, bacteria, and fungi exhibit a similar color change⁴⁹. The brown color of AgNPs is caused by the excitation of surface plasmon resonance in silver metal nanoparticles. The SPR is an optical phenomenon in which electrons in the conduction band on the surface of AgNPs oscillate collectively in resonance with the light wave, resulting in high absorption and scattering⁵⁰. These resonances occur only in metallic AgNPs, not in bulk metallic particles. As a result, the color change is the primary indicator of AgNP formation.

Furthermore, the formation of AgNPs was identified through UV-Vis absorption spectrum scanning in the range of 300-800 nm. Typically, all biosynthesized AgNPs exhibited a single absorption peak around 420 nm, which corresponded to the SPR peak of AgNPs. At the same time, no absorption band is visible with either plant extract or AgNO₃ solution (Figure 1b). Absorption peaks at this wavelength are commonly associated with silver nanoparticles, typically ranging in size from 2 to 100 nm⁵¹. Mie's theory posits that a single absorption band noted in the UV-Vis spectra is indicative of the construction of spherical nanoparticles, whereas multiple SPR bands reveal the presence of other anisotropic forms⁵². Given this theory, we propose that the AgNPs obtained herein are spherical, and SEM and TEM microscopy support this conclusion.

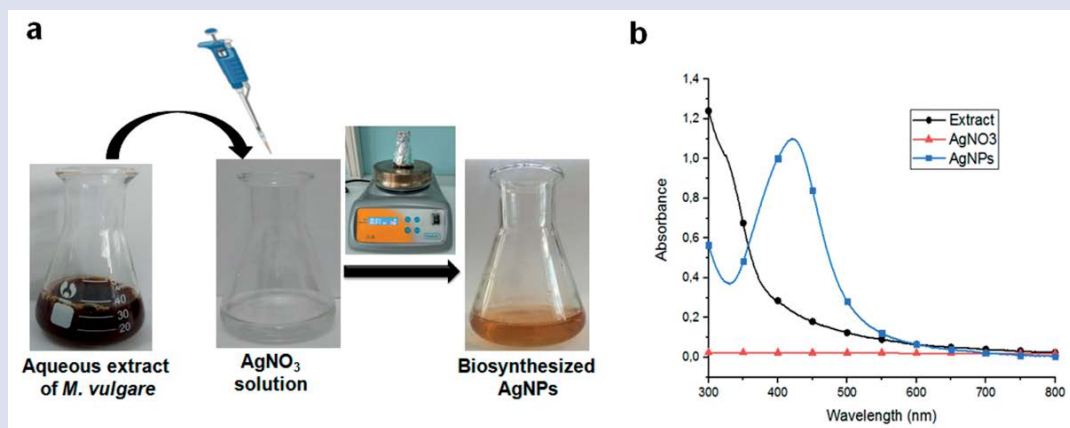


Figure 1: (a) Color change image and (b) UV-visible absorption spectra of *M. vulgare* extract, AgNO_3 , and AgNPs.

Optimization of reaction parameters

The size, shape, and dispersity of the formed AgNPs have a representative effect on the position, width, and shape/intensity of the SPR band. The position and width of the SPR peak provide detailed information on the size of nanoparticles during synthesis process optimization; the appearance of a broad peak at a higher wavelength suggests particle size enlargement, while a narrow peak at a shorter wavelength indicates a decrease in particle size⁴⁰. Meanwhile, the peak intensity is reciprocal to the concentration of nanoparticles produced in the reaction medium. Numerous studies have shown that the synthesis of shape- and size-controlled AgNPs can be achieved by optimizing reaction parameters, including temperature and silver nitrate concentration, extract volume, and reaction time. Therefore, these four parameters were investigated and optimized.

Effect of temperature on AgNPs synthesis

The temperature of the reaction plays a crucial role in affecting the reaction rate during the synthesis process and the characteristics of AgNPs. The influence of temperature on AgNP formation was studied by incubating the reaction mixtures at various temperatures: from 20 °C to 80 °C with intervals of 10 °C, while maintaining the reactant and reductant concentrations constant. Figure 2a shows that *M. vulgare* mediated the production of silver nanoparticles at various reaction temperatures, with the highest SPR peak intensity detected at 80 °C. At relatively low temperatures (20 °C and 30 °C), the samples exhibited broad SPR bands with weak intensity, indicating the formation of a small number of large AgNPs. However, a notable increase in the absorbance of AgNPs was observed as the reaction temperature escalated from 40 °C to 80 °C, and SPR peaks became sharper and shifted slightly toward shorter wavelengths, indicating the formation of a large number of small-sized nanoparticles. Many studies have found that high temperatures promote a fast nucleation process, resulting in the formation of more nuclei through the rapid consumption of reactants and preventing any secondary reduction on the surface of the preformed nuclei⁵³. As a result, small AgNPs were formed at high temperatures. Subsequent experiments were carried out at 80 °C.

Effect of AgNO_3 concentration on AgNPs synthesis

The impact of AgNO_3 concentration on the reduction of silver metal ions was studied by homogenizing 0.1 mL of plant extract with AgNO_3 solutions of varying concentrations (0.25 to 4 mM), while the reaction mix was stirred at 80°C for 1 hour. Results in Figure 2b show that the intensity of the SPR peak gradually increases as AgNO_3 concentrations increase from 0.25 to 2 mM, indicating that AgNPs are produced in abundance. Furthermore, as the AgNO_3 concentration increased

from 0.25 to 2 mM, the SPR peaks gradually shifted from 439 nm to 420 nm, possibly due to a reduction in the particle size of AgNPs. However, by increasing the AgNO_3 concentration to 3 mM or higher, the absorption intensity of the SPR peak decreased significantly. This decrease indicates a lower yield of AgNPs due to agglomeration. The data show that 2 mM of AgNO_3 is the optimal concentration for AgNP synthesis. Above this concentration, a large number of AgNPs were produced, increasing the collisions between silver nanoparticles and causing their aggregation. Tamilarasi et al. also discovered that a two mM concentration was optimal for silver nanoparticle biosynthesis using *Gomphrena globosa* leaf extract and that the yield of AgNPs decreased as AgNO_3 concentrations increased to 3-5 mM⁵⁴.

Effect of extract volume on AgNPs synthesis

Serving as a reducing and stabilizing agent, the plant extract is crucial in the synthesis of AgNPs and can modulate both particle size and morphology. Figure 2c depicts the variation in the absorption spectra of AgNPs synthesized at 80 °C for 1 h with different volumes of *M. vulgare* extract and 2 mM AgNO_3 solution. Nanoparticles were successfully synthesized at all test extract volumes. Increasing the extract concentration from 50 to 100 μL intensifies the SPR bands without shifting their positions. Increasing the extract concentration from 200 to 700 μL led to increased absorption intensity and a broader absorption band shape. The λ_{max} was red-shifted from 428 to 437 nm. These findings were due to an increase in the particle size of AgNPs. The optimal volume for stabilizing AgNPs was 100 μL of extract. The increase in AgNP size at volumes above the optimum is due to *M. vulgare* extract's high reducing capacity, which promotes the secondary reduction of silver metal ions on the nuclei's surface. The results show that *M. vulgare* extract has excellent reducing potential, even at a low volume of 100 μL . A previous study on the synthesis of AgNPs with *Indian belladonna* extract found a similar increase in AgNP size with increasing extract volume. *Indian belladonna* leaf extract has a high reduction potential, even at a low volume of 200 μL ¹⁶.

Effect of reaction time on AgNPs synthesis

Reaction time is another important factor that influences AgNPs biosynthesis. The effect of reaction time was assessed at various time intervals while other parameters remained constant. Figure 2d shows that AgNPs began to form within 5 min of adding *M. vulgare* extract to an AgNO_3 solution. The intensity of the SPR peak increased gradually over time, indicating the formation of more AgNPs. This trend can be attributed to the rapid nucleation and formation of AgNPs at 80 °C. It was also observed that the wavelength of maximum absorbance (λ_{max}) changed negligibly with time, implying that the nanoparticles

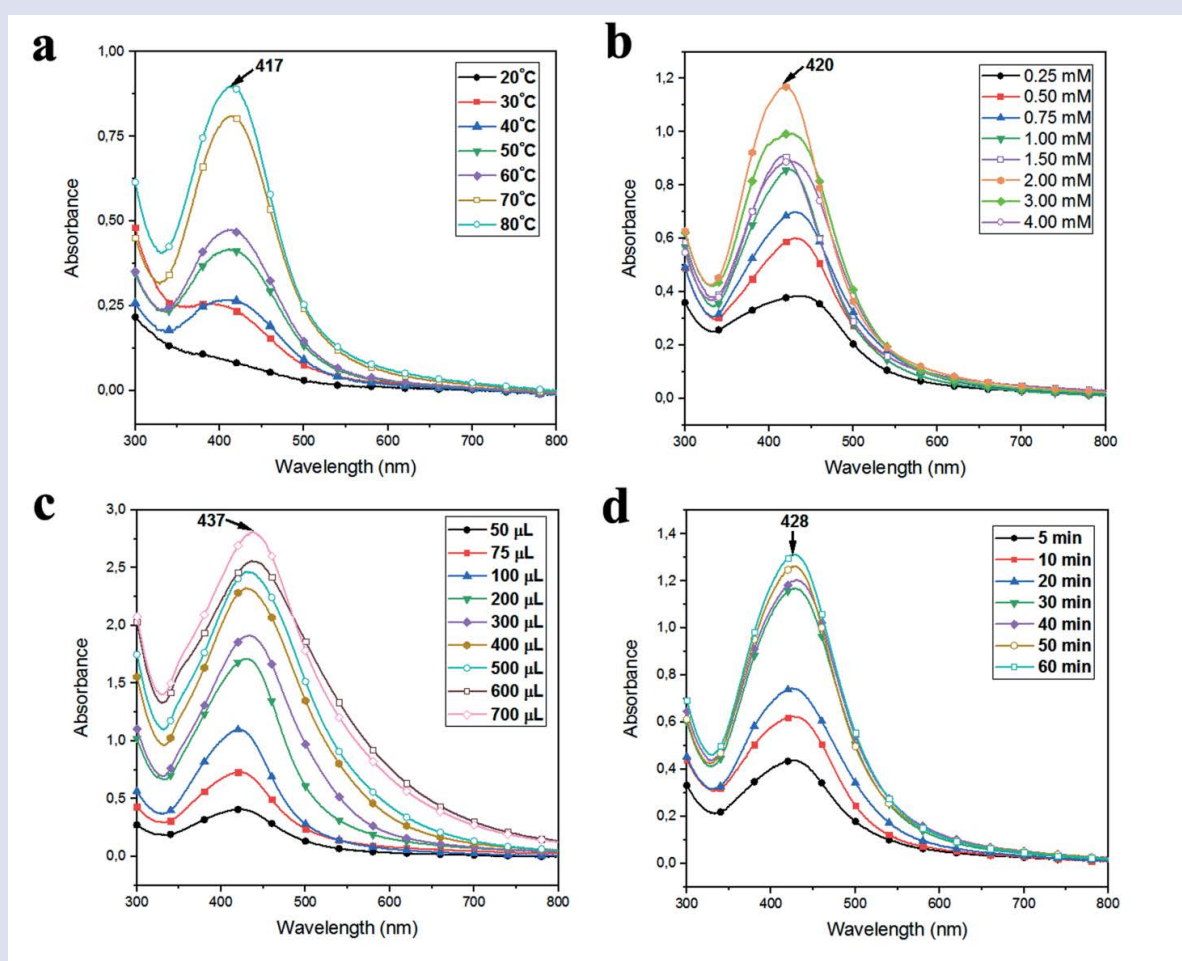


Figure 2: UV-visible absorption spectra of biosynthesized AgNPs. Effect of (a) temperature, (b) concentration of AgNO_3 , (c) extract volume, and (d) time on the synthesis of AgNPs.

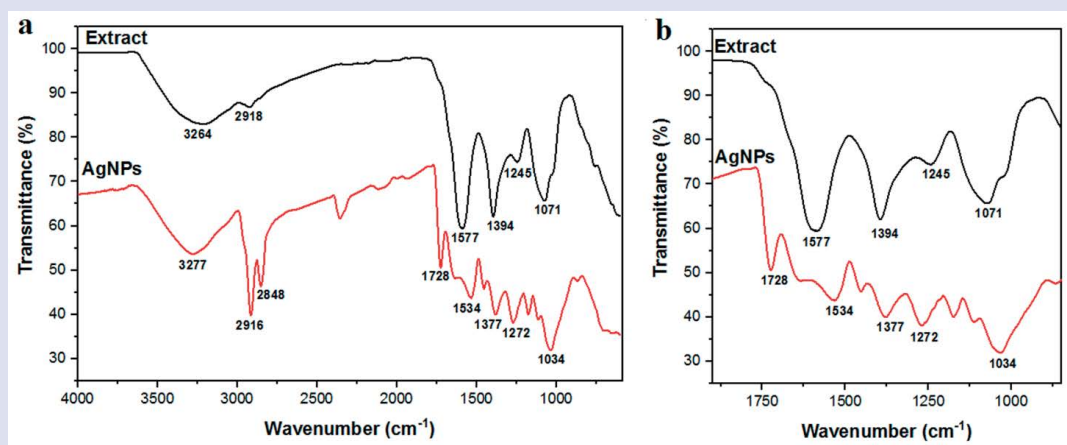


Figure 3: (a) FTIR spectra of pure *M. vulgare* leaf extract and phytofabricated AgNPs and (b) zoomed spectra in the wavenumber range of 850 to 1900 cm^{-1} .

were homogeneous and nearly the same size. The high reducing capacity of the active components in *M. vulgare* extract causes the rapid generation of AgNPs. After 60 min, there was no further change in absorption intensity, indicating that the *M. vulgare* aqueous extract had completely reduced the silver salt. As a result, the optimal reaction time for AgNP synthesis was determined to be 60 min. Many studies

have shown that AgNP biosynthesis is time-dependent. However, the optimal synthesis durations frequently differ between studies, owing to the nature and amount of reducing phytoconstituents present in different plant extracts, as well as differences in AgNP production conditions.

AgNP characterization

FTIR analysis

The major functional groups involved in silver bioreduction and AgNP capping were identified using FTIR analysis. As a result, the FTIR spectra of *M. vulgare* extract and as-synthesized AgNPs, shown in Figure 3, were compared. The IR spectrum of *M. vulgare* extract revealed multiple peaks, indicating the plant's complexity. The band at 3264 cm^{-1} is related to the O-H stretching vibration characteristic of phenols or alcohols, while the band at 2918 cm^{-1} is associated with the C-H stretching mode found in alkanes. Additionally, the peak at 1577 cm^{-1} is linked to aromatic C=C stretching, and the peak at 1394 cm^{-1} arises from the bending vibrations of O-H in carboxylic acids. The peak at 1245 cm^{-1} is corresponding to the C-N stretching of amines, whereas the absorption peak at 1071 cm^{-1} indicates C-O stretching associated with primary alcohols. Finally, signals detected between 800 and 600 cm^{-1} are most likely related to alkyl halides⁵⁵. A detailed assessment of the plant extract spectrum indicated the existence of terpenoids, alkaloids, polyphenols, flavonoids, and phenolic acids, as well as other phytochemicals known for their reducing and stabilizing capabilities. The representative spectrum of AgNPs exhibited a similar spectral pattern to the *M. vulgare* extract with marginal shifts, indicating that the biomolecules' functional groups interacted with the AgNPs' surface. The absorption peaks were found at 3277 , 2916 , 1534 , 1377 , 1272 , and 1034 cm^{-1} . A new band centered at 1728 cm^{-1} emerged in the FTIR spectrum of AgNPs. This finding points to the formation of the carbonyl C=O group, demonstrating that Ag⁺ was reduced by specific hydroxyl groups that were oxidized to carbonyl groups^{56,57}.

XRD analysis

XRD was used to determine the crystalline nature of the synthesized AgNPs. In Figure 4, an XRD pattern is shown with four prominent diffraction peaks at 2θ values of 38.22° , 46.18° , 64.27° , and 77.16° . These peaks refer to the (111), (200), (220), and (311) reflection planes of silver's face-centered cubic crystalline structure. These findings are consistent with those from previous studies^{16,58}. In addition to the Bragg peaks typical of silver nanocrystals, the recorded XRD pattern displayed additional peaks at 27.86° , 32.14° , 54.84° , and 57.45° . These peaks may represent biomolecules derived from *M. vulgare*'s aqueous extract. Okaiyeto et al. and Sithara et al. found similar results and concluded that the additional peaks are caused by phytochemical compounds present in the plant's aqueous extract coating and stabilizing the surface of the synthesized AgNPs^{59,60}.

Particle size and PDI determination

DLS determined the average particle size and polydispersity index (PDI) of nanoparticles, as shown in Figure 5. *M. vulgare* produced AgNPs with an average particle size of 34.58 nm and a PDI value of 0.250 , indicating that under optimal reaction conditions, small-sized AgNPs formed, which is consistent with UV-visible spectroscopy results. DLS revealed a low PDI value, indicating good AgNP monodispersity. In general, nanoparticles are considered monodisperse when their PDI is lower than 0.3 ⁶¹. Previous studies have also found small nanoparticle sizes and low PDI values for AgNPs produced by plants^{20,62}.

Morphological features and EDX analysis

SEM was performed to analyze the surface morphology and size of well-designed AgNPs in the solid phase. The SEM image (Figure 6a) shows a few small spherical silver nanoparticles with a diameter of less than 50 nm , highlighted in red circles. It also shows that the sample is composed of highly agglomerated nanoparticles that have primarily formed large aggregates with no well-defined morphology. This agglomeration could be due to the drying process. According to Tung et al., during the drying process, water molecules flow from the

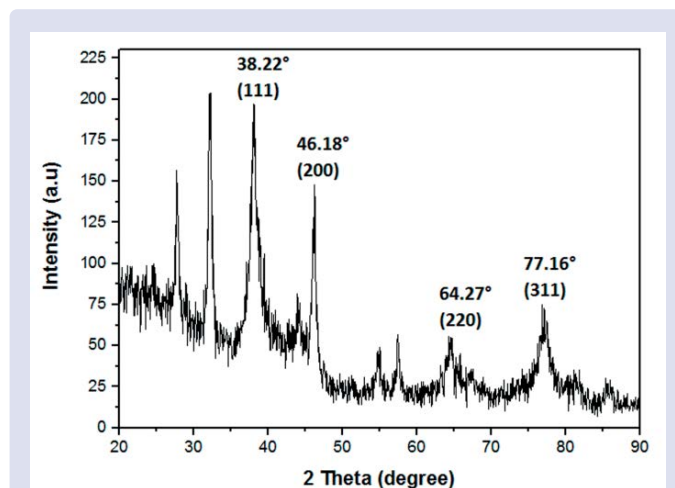


Figure 4: XRD diffractogram of the AgNPs biosynthesized using *M. vulgare* leaves extract.

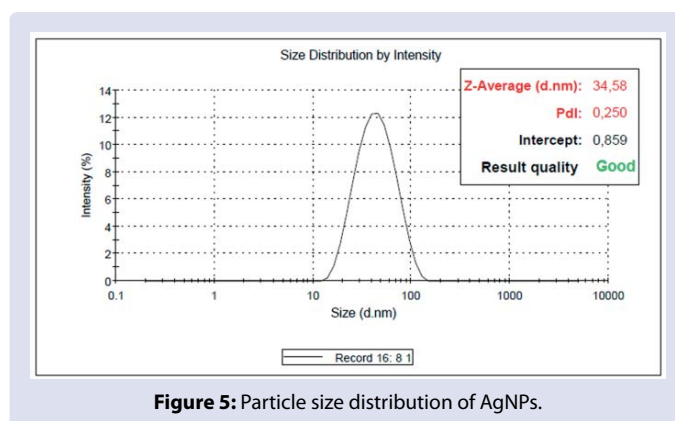


Figure 5: Particle size distribution of AgNPs.

droplet's center to its edge, causing solid particles to be dragged and agglomerated at the periphery⁶³. Furthermore, residual precursors absorbed on the surface of AgNPs may cause inter-particle necking, resulting in the formation of agglomerates.

The AgNPs were also analyzed using EDX, and the resulting profile is shown in Figure 6b. A strong characteristic peak at 3 keV was detected, confirming the presence of an elemental silver signal from silver nanoparticles. The remaining minor signal peaks are most likely caused by elements that served as a capping agent and were bound to the surface of AgNPs. TEM analysis was utilized to clarify the morphology and size of the particles. Figure 6c depicts the morphology of the nanoparticles as revealed by TEM. The synthesized AgNPs had a size of less than 50 nm and a spherical shape. Prior research conducted by Lupuliasa et al. also described the obtention of spherical AgNPs synthesized using aerial parts of *M. vulgare*³⁸.

Antimicrobial susceptibility testing

Agar well diffusion assay

Using a well diffusion test on an agar plate, the antimicrobial activities of the aqueous extract of *M. vulgare*, AgNO_3 , and AgNPs were assessed at different concentrations (10 , 25 , 50 , 75 , and $100\text{ }\mu\text{L}$) against a selection of microorganisms. The presence of clear inhibitory zones around the wells confirmed the tested compounds' growth-inhibitory effect. Interestingly, the results shown in Figures 7 and 8 show that the biosynthesized AgNPs exhibited remarkable antimicrobial activity against all tested microorganisms, with bacteria being more susceptible

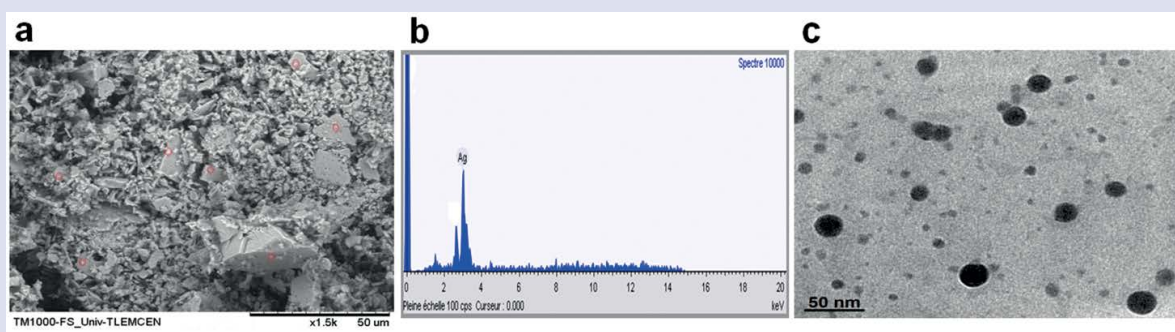


Figure 6: (a) The SEM image of biosynthesized AgNPs, (b) EDX profile of AgNPs, and (c) TEM micrograph of synthesized AgNPs from *M. vulgare* leaves extract.

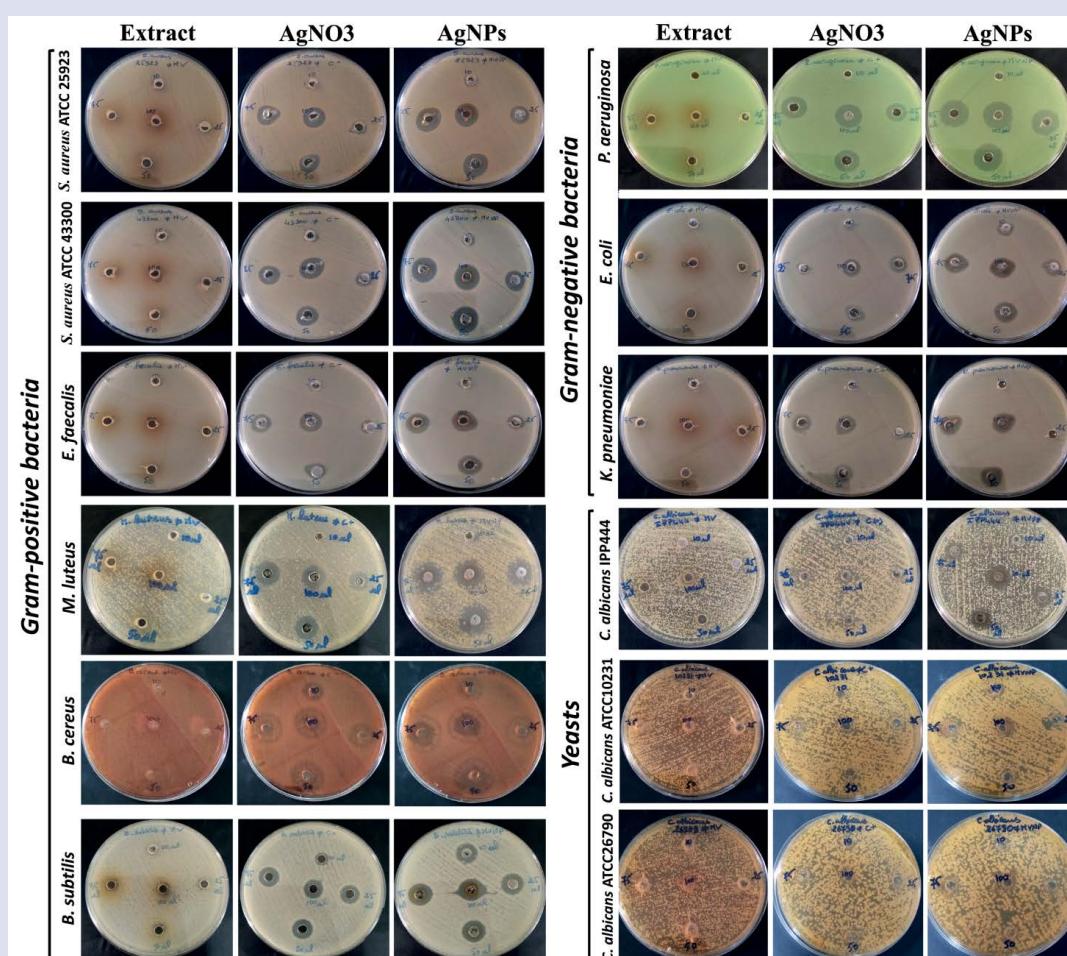


Figure 7: Plates showing the zones of inhibition (mm) of AgNPs, AgNO₃ and *M. vulgare* extract against various microorganisms at different concentrations.

than yeasts. At a dose of 100 μL, *M. luteus* was the most inhibited bacterial strain with ZOI of 19.50±0.50 mm, followed by *P. aeruginosa* (ZOI-18.33±0.58 mm), *S. aureus* MRSA (ZOI-17±0.0 mm), and *S. aureus* MSSA (ZOI-15.83±0.29 mm). For other tested bacterial strains, ZOI for AgNPs at a dose of 100 μL ranged between 13.00 and 15 mm.

At a dose of 100 μL, AgNPs stopped the development of *C. albicans* IPP444 strains by an inhibition zone of 13.66±0.58 mm. However, no growth inhibition was observed with *C. albicans* ATCC 26790 or *C. albicans* ATCC 10231. Figures 7 and 8 also show that AgNO₃ antimicrobial inhibition potential against all tested pathogens was

lower than that induced by AgNPs at all strengths. However, the results show that the plant extract did not inhibit the growth of the tested bacteria and yeasts. This finding implies that the aqueous extract had no antimicrobial effect on its own, which could be explained by the low extract concentration used in the experiment. According to Balashanmugam, the extract from *Cassia roxburghii* used for AgNP synthesis does not affect the growth of *P. aeruginosa*, *E. coli*, *B. subtilis*, *S. aureus*, and *M. luteus*⁶⁴. In this study, the results show that AgNPs had a dose-dependent antimicrobial effect against all tested microbial strains in the concentration range of 10-100 μL. The highest cytotoxic

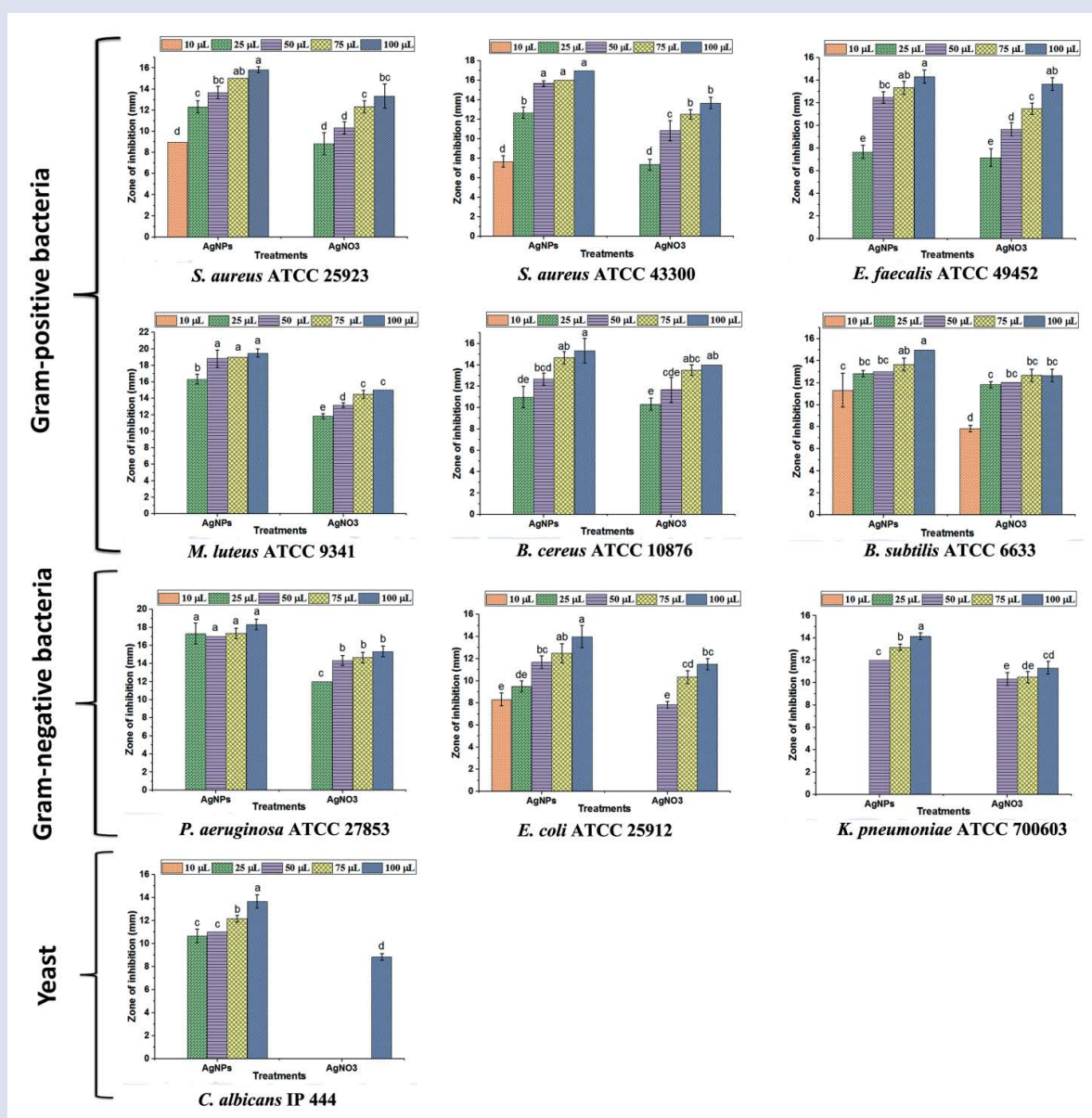


Figure 8: Bar graph showing the inhibition zone diameters induced by AgNPs and AgNO₃ against selected microbial strains. Data are expressed as mean ± SD (n=3). Different letters denote significant differences between groups within microbial species based on Tukey's test (p-value < 0.05).

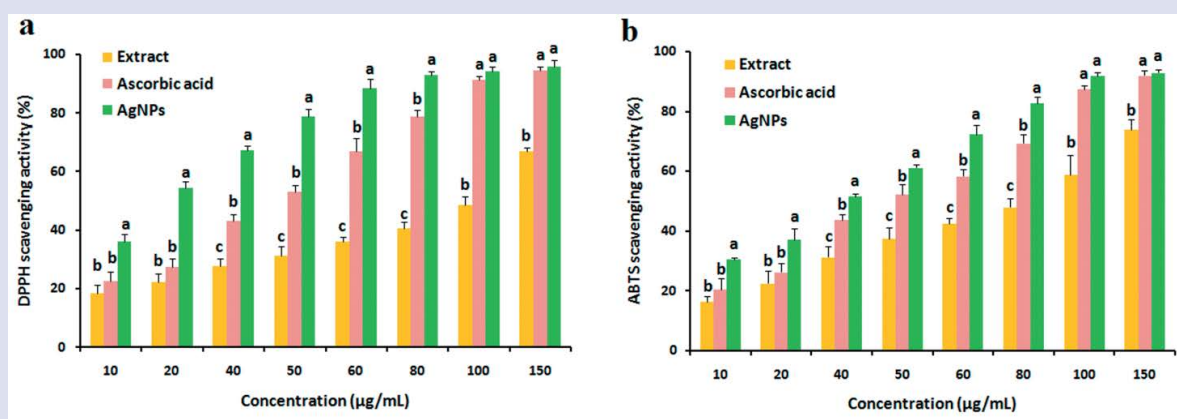


Figure 9: Antioxidant activity of AgNPs, *M. vulgare* extract, and ascorbic acid assessed using DPPH assay (a) and ABTS assay (b). Different letters in the same concentration indicate the data are significant (p < 0.05).

effect was observed with 100 µL of AgNPs, aligning with the findings reported by Ali et al⁶⁵.

Research has shown that the thinner peptidoglycan layer found in the cell walls of Gram-negative bacteria contributes to their unique characteristics; AgNPs are more effective at inhibiting them than Gram-positive bacteria. Unlike the findings of these groups, this study did not demonstrate a greater inhibitory potency against Gram-negative bacteria. Indeed, the AgNPs synthesized from *M. vulgare* revealed representative antibacterial potential against both Gram bacteria, particularly *M. luteus*, *P. aeruginosa*, and *S. aureus* MRSA. This evidence is in agreement with the findings of Skandalis et al. and Enerelt Urnukhsaikhan et al., who indicated that the antimicrobial strength of AgNPs operates independently of cell wall composition^{48,66}. The agar well diffusion assay also evidenced a non-negligible anticandidal activity of AgNPs against *Candida albicans* IPP444.

It should be noted that although many studies have tested the antibacterial potency of AgNPs, few studies have explored their inhibitory effect against yeasts of the *Candida* genus. He et al. used longan peel extract for the synthesis of AgNPs and reported moderate antimicrobial activity on *Candida albicans* ATCC 10231⁶⁷. In previous studies, AgNPs produced by *Syzygium cumini*⁶⁸, *Caesalpinia ferrea*⁶⁹, *Cassia roxburghii*⁶⁴, *Hyptis suaveolens*⁷⁰, and other species were shown to have antifungal activity against various fungal species. Overall, preliminary antimicrobial screening revealed that AgNPs successfully suppressed the growth of all bacteria evaluated and *Candida albicans* IPP444. As a result, the AgNPs developed herein have the potential to be a promising antimicrobial agent capable of overcoming current microbial resistance.

MIC, MBC and MFC determination

To achieve more accurate and precise data on the antimicrobial attribute of the tested AgNPs, AgNO₃, and standard drugs, the MIC,

MBC, and MFC were determined (Table 1). The MIC values for AgNPs ranged from 0.041 to 5.312 µg/mL, while those for AgNO₃ ranged from 0.083 to 10.62 µg/mL against all tested bacterial strains. Levofloxacin, a broad-spectrum antibiotic, effectively suppressed the growth of all selected bacterial strains, with MIC values varying between 0.015 and 0.976 µg/mL. The results showed that AgNPs and AgNO₃ were active against yeasts with MICs of 2.656 µg/mL and 5.312 µg/mL, respectively. The MIC values for amphotericin B ranged from 2 to 8 µg/mL. Interestingly, for *C. albicans* ATCC 10231 and *C. albicans* IP444, AgNPs had lower MIC values than amphotericin B. The results show that the synthesized AgNPs exhibited higher activity than AgNO₃.

AgNPs, on the other hand, inhibited all microorganism growth at low concentrations, supporting the findings of the well diffusion test. Several studies reported similar findings, highlighting AgNPs' potent antimicrobial activity against a wide range of microbial species^{43,71}. Notably, the MIC values of the AgNPs obtained herein are lower than those reported in some studies for plant-based AgNPs of comparable size^{72,73}. Given the lack of ideal standardized methods for assessing the antimicrobial propensity of biosynthesized AgNPs, we believe it will be difficult to compare our findings to all MIC values reported in other studies. Variations in initial microbial concentration, microbial strains, culture media composition, and various other factors are critical in determining antimicrobial activity. Additionally, aspects like size, shape, surface charge, and capping agents can also influence the antimicrobial performance of AgNPs.

The MBC and MFC values of AgNPs were equal to or two-fold greater than those of the corresponding MIC values against all microorganisms tested, except for *K. pneumoniae* ATCC 700603, where the MBC value was determined to be four-fold higher than the MIC. Consequently, the MBC/MIC and MFC/MIC ratios were ≤ 4, revealing that AgNPs were bactericidal and fungicidal. For AgNO₃, bactericidal, bacteriostatic, and fungicidal activities were generally

Table 1: MICs, MBCs, MFCs, and MBC (or MFC)/MIC ratios of AgNPs, AgNO₃, and standard drugs against 12 microorganisms.

Microorganisms	MIC (µg/mL)			MBC (or MFC) (µg/mL)			MBC (or MFC)/MIC		
	AgNPs	AgNO ₃	LEV/AmpB	AgNPs	AgNO ₃	LEV/AmpB	AgNPs	AgNO ₃	LEV/AmpB
Gram-positive bacteria									
<i>S. aureus</i> ATCC 25923	0.041	0.083	0.015	0.083	0.664	0.061	2	8	4
<i>S. aureus</i> ATCC43300	1.328	2.656	0.122	1.328	2.656	0.122	1	1	1
<i>E. faecalis</i> ATCC 49452	1.328	2.656	0.244	1.328	2.656	0.976	1	1	4
<i>M. luteus</i> ATCC 9341	0.083	0.332	0.122	0.166	0.664	0.976	2	2	8
<i>B. cereus</i> ATCC 10876	0.332	0.664	0.061	0.332	0.664	0.488	1	1	8
<i>B. subtilis</i> ATCC 6633	1.328	2.656	0.122	2.656	10.625	0.976	2	4	8
Gram-negative Bacteria									
<i>P. aeruginosa</i> ATCC 27853	5.312	10.625	0.976	5.312	21.250	1.953	1	2	2
<i>E. coli</i> ATCC 25912	0.664	2.656	0.244	1.328	2.656	0.488	2	1	2
<i>K. pneumoniae</i> ATCC 700603	1.328	2.656	0.488	5.312	2.656	0.976	4	1	2
Yeasts									
<i>C. albicans</i> ATCC 10231	2.656	5.312	8	5.312	5.312	8	2	1	1
<i>C. albicans</i> ATCC 26790	2.656	5.312	2	2.656	10.625	4	1	2	2
<i>C. albicans</i> IPP444	2.656	5.312	4	2.656	10.625	8	1	2	2

Table 2: Anti-inflammatory activity of sodium diclofenac, *M. vulgare* extract, and AgNPs.

Concentration µg/mL	Percent inhibition		
	Sodium diclofenac	AgNPs	<i>M. vulgare</i> extract
12,50	11.47±1.41 ^a	09,65±1.12 ^a	5.25±0.75 ^b
25	28.01±1.62 ^a	20.25±2.07 ^b	13.72±1.80 ^c
50	45.43±1.21 ^a	37.54±0.77 ^b	27.48±0.64 ^c
75	65.59±1.12 ^a	55.04±0.88 ^b	46.68±0.65 ^c
100	95.86±0.16 ^a	78.40±1.00 ^b	65.70±1.21 ^c
200	97.17±0.35 ^a	86.14±1.78 ^b	72.59±0.81 ^c
IC50 (µg/mL)	53.31±0.71	65.35±0.64	79.15±1.10

Values are expressed as mean ± SD. Different letters in the same concentration indicate the data are significant ($p < 0.05$).

shown. This potent antimicrobial activity is primarily due to the small size of the synthesized AgNPs. Indeed, a large number of studies discovered that controlling AgNP size was critical for achieving the best bactericidal and fungicidal response^{74,75}. Smaller nanoparticles with a higher surface-to-volume ratio are more toxic to microbial pathogens than their larger counterparts. Therefore, we speculate that the small AgNPs developed in this study could easily penetrate microbial cells, and induce structural modifications in the cell envelope, which can eventually lead to cell death.

In addition to particle size, AgNPs' spherical shape may have influenced their antimicrobial efficacy by facilitating interactions with microorganisms. Numerous studies have demonstrated that small-sized spherical AgNPs have higher antibacterial efficacy than triangular, disk, or large spherical-shaped AgNPs^{75,76}. Aside from size and shape, the concentration of AgNPs significantly influenced antimicrobial activity and was unique to each microbial strain tested. It is worth noting that the small size of the AgNPs obtained in this study resulted in low MIC, MBC, and MFC values, which is consistent with previous findings^{77,78}. Therefore, based on the findings, it can be noted that AgNPs synthesized with *M. vulgare* exhibited broad-spectrum microbicidal activity against the twelve tested microbial strains.

Despite the extensive literature on AgNPs' antimicrobial properties, the exact mechanism underlying their effect has yet to be fully understood. There have been four well-defined mechanisms proposed thus far: (i) irreversible damage of microbial cell membrane as a result of the accumulation and adhesion of AgNPs on the cell surface; (ii) the uptake of AgNPs into microbial cells leads to the disruption of intracellular organelles (like vacuoles, mitochondria, and ribosomes) and biomolecules (such as enzymes, lipids, proteins, and DNA), as well as (iii) an increase in the intracellular concentration of reactive oxygen species (ROS) and free radicals, leading to induced cellular toxicity and oxidative stress; and (iv) modulation of signal transduction pathways⁷⁹. Thus, all these mechanisms can often be combined to produce potent antimicrobial activity.

Antioxidant activity

The results of the DPPH and ABTS experiments revealed that all compounds tested had antioxidant activity (Figure 9). There was an increase in antioxidant activity that correlated with the doses tested. AgNPs and ascorbic acid at 150 µg/mL showed maximum scavenging activity of 95.83±2.10 % and 94.53±1.14 % with the DPPH assay, respectively, while the extract inhibited the DPPH radical by 66.84±1.25 % at the same concentration. It was revealed that at concentrations varying from 10 to 80 µg/mL, the free radical scavenging activity of the biosynthesized AgNPs was notably superior to that of the reference drug, ascorbic acid. The IC50 values recorded for AgNPs, ascorbic acid, and extract were 20.81±2.09 µg/mL, 45.59±2.38 µg/mL, and 103.44±4.66 µg/mL, respectively. In the ABTS assay, at concentrations varying from 10 to 150 µg/mL, the biogenic AgNPs displayed an activity range of 30–92% compared to the extract, which exhibited

16–73% capacity to scavenge free radicals. AgNPs showed a more elevated free radical scavenging activity than ascorbic acid and the aqueous extract used for their synthesis. These findings fit well with the study of Dubey et al., which demonstrated that the antioxidant activity of AgNPs exceeded that of *Woodfordia fruticosa* extract and ascorbic acid⁸⁰. The extract's antioxidant activity largely arises from the secondary metabolites found within the plant, which act as hydrogen or electron donors responsible for DPPH and ABTS reduction. For AgNPs, this remarkable activity is due, on the one hand, to their catalytic effect and, on the other hand, to the capped biomolecules that act as antioxidant agents⁸¹. Additionally, the elevated surface-to-volume ratio of the biosynthesized nanoparticles may have enhanced their ability to interact with and neutralize reactive oxygen species. Overall, these nanoparticles can be utilized as antioxidant agents to protect human health against diseases caused by oxidative stress.

Anti-inflammatory activity

Inflammation refers to the vital human body's defensive response to protect itself against stimuli it recognizes as potentially harmful. It occurs mainly in two phases: an initiation phase and an adequate resolution phase⁸². The inflammatory response is complex and involves an orchestrated cascade of interactions among inflammatory mediators that aims to restore tissue homeostasis. However, unresolved inflammation and persistence of the inflammatory phase may lead to tissue damage, prompting the development of chronic inflammatory diseases⁸³. Although commonly used chemical drugs to manage inflammatory conditions are potent, their long-term use is associated with harmful impacts on health⁸⁴. In search of new anti-inflammatory drugs with fewer adverse events, biogenically synthesized AgNPs are emerging as a reliable natural alternative for the resolution of inflammation. It is well-documented that protein denaturation correlates with the occurrence of the body's inflammatory response⁸⁵. Therefore, agents endowed with the ability to prevent protein denaturation would be promising candidates for anti-inflammatory drug development. The anti-inflammatory potential of *M. vulgare* extract and biosynthesized AgNPs was evaluated using the albumin denaturation assay. Table 2 depicts the percentage inhibition values of protein denaturation obtained with tested compounds.

Results revealed that biosynthesized AgNPs and *M. vulgare* extract could prevent heat-induced albumin denaturation at all tested concentrations. The percent inhibition of diclofenac sodium reached 97.17% at 200 µg/mL of concentration, whereas the percent inhibition of AgNPs and *M. vulgare* leaf extract were 86.14% and 72.59%, respectively. The lowest percentage inhibition of albumin denaturation for diclofenac sodium, AgNPs, and the extract were recorded at 12.5 µg/mL. AgNPs exerted a significantly ($p < 0.05$) higher inhibition of albumin denaturation at all tested concentrations compared to *M. vulgare* extract. These findings clearly suggest that AgNPs synthesized using *M. vulgare* possess promising anti-inflammatory properties.

Recent research indicates that the aqueous leaf extract of *M. vulgare* exhibits significant anti-inflammatory properties⁸⁶. We speculate that the protection of BSA from heat denaturation is probably due to interactions between the protein and the AgNPs. These interactions may be electrostatic or hydrophobic in nature. Forces such as Van der Waal's forces may also be involved⁸⁷. Further investigations are needed to clarify the underlying mechanisms behind the anti-inflammatory effect of AgNPs.

CONCLUSION

In this study, we successfully synthesized biogenic AgNPs via the green route using *M. vulgare* aqueous leaf extract. The plant extract was high in phenolic compounds, which may have served as reducing and stabilizing agents during the synthesis process. Temperature, AgNO₃ concentration, extract volume, and reaction time were among the synthesis parameters investigated and optimized. AgNP formation was validated through visual color changes and the detection of an SPR peak at 420 nm in the UV-visible spectrum. Additionally, SEM/TEM and DLS analyses demonstrated that the biosynthesized AgNPs were uniformly distributed and spherical, averaging 34.58 nm in size.

Moreover, the XRD pattern indicated the crystalline nature of AgNPs, while the FTIR spectra revealed that biomolecules found in *M. vulgare* extract are primarily responsible for AgNP reduction, capping, and stabilization. At low concentrations, these biogenic AgNPs demonstrated significant antimicrobial efficacy against every microbial strain examined. Therefore, the microbicidal effect of AgNPs makes them a promising candidate for future microbial infection control. Further research is required to decipher the mechanism of action of AgNPs against pathogenic microorganisms and to assess their in vivo efficacy. The DPPH and ABTS assays revealed the potent antioxidant activity of AgNPs. Additionally, AgNPs showed potent in vitro anti-inflammatory activity by inhibiting albumin denaturation. *M. vulgare* can be a fast, economical and environmentally friendly alternative for generating antimicrobial, antioxidant and anti-inflammatory AgNPs in one step. Further investigations should focus on the analysis of the chemical composition of the aqueous extract and the evaluation of the cytotoxicity, in vivo effects and the mechanisms of action behind the biological activities of the biosynthesized AgNPs.

CONFLICTS OF INTEREST

The authors declare that they have no conflicts of interest.

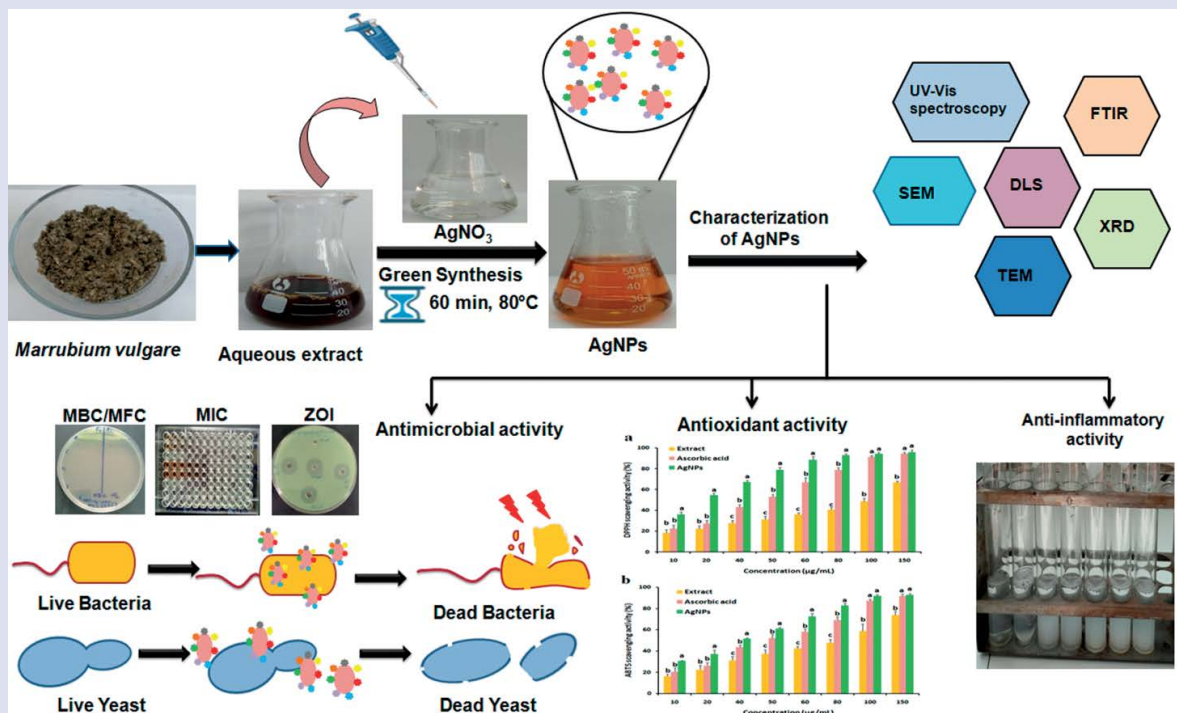
REFERENCES

- Joudeh N, Linke D. Nanoparticle classification, physicochemical properties, characterization, and applications: a comprehensive review for biologists. *J. Nanobiotechnology*. 2022;20:1-29.
- Otoni CA, Simões MF, Fernandes S, Dos Santos JG, Da Silva ES, de Souza RFB, et al. Screening of filamentous fungi for antimicrobial silver nanoparticles synthesis. *AMB Express*. 2017;7:1-10.
- Zhang X-F, Liu Z-G, Shen W, Gurunathan S. Silver nanoparticles: synthesis, characterization, properties, applications, and therapeutic approaches. *Int. J. Mol. Sci*. 2016;17:1534.
- Bruna T, Maldonado-Bravo F, Jara P, Caro N. Silver nanoparticles and their antibacterial applications. *Int. J. Mol. Sci*. 2021;22:7202.
- Mahiuddin M, Saha P, Ochiai B. Green synthesis and catalytic activity of silver nanoparticles based on Piper chaba stem extracts. *Nanomaterials*. 2020;10:1777.
- Marinescu L, Ficai D, Ficai A, Oprea O, Nicoara AI, Vasile BS, et al. Comparative Antimicrobial Activity of Silver Nanoparticles Obtained by Wet Chemical Reduction and Solvothermal Methods. *Int. J. Mol. Sci*. 2022;23:5982.
- Lotfy WA, Alkersh BM, Sabry SA, Ghozlan HA. Biosynthesis of silver nanoparticles by *Aspergillus terreus*: characterization, optimization, and biological activities. *Front. bioeng. biotechnol*. 2021:265.
- Pérez de la Lastra JM, Anand U, González-Acosta S, López MR, Dey A, Bontempi E, et al. Antimicrobial resistance in the COVID-19 landscape: is there an opportunity for anti-infective antibodies and antimicrobial peptides? *Front. Immunol*. 2022:2698.
- Murray CJ, Ikuta KS, Sharara F, Swetschinski L, Aguilar GR, Gray A, et al. Global burden of bacterial antimicrobial resistance in 2019: a systematic analysis. *Lancet*. 2022;399:629-655.
- Razzaque MS. Exacerbation of antimicrobial resistance: another casualty of the COVID-19 pandemic? *Expert Rev. Anti Infect. Ther*. 2021;19:967-971.
- Antimicrobial resistance. <https://www.who.int/news-room/fact-sheets/detail/antimicrobial-resistance>.
- Abimbola SO, Otieno MA, Cole J. Reducing the use of antimicrobials as a solution to the challenge of antimicrobial resistance (AMR): approaching an ethical dilemma through the lens of planetary health. *Challenges*. 2021;12:23.
- Gao W, Zhang L. Nanomaterials arising amid antibiotic resistance. *Nat. Rev. Microbiol*. 2021;19:5-6.
- Javed MA, Ali B, Sarfraz MH, Ali S, Liaqat E, Afzal MS, et al. Biosynthesis and characterization of silver nanoparticles from *Cedrela toona* leaf extracts: An exploration into their antibacterial, anticancer, and antioxidant potential. *Green Processing and Synthesis*. 2024;13:20230248.
- Fafal T, Taştan P, Tüzün B, Ozyazici M, Kivcak B. Synthesis, characterization and studies on antioxidant activity of silver nanoparticles using *Asphodelus aestivus* Brot. aerial part extract. *S. Afr. J. Bot*. 2017;112:346-353.
- Rajput S, Kumar D, Agrawal V. Green synthesis of silver nanoparticles using Indian *Belladonna* extract and their potential antioxidant, anti-inflammatory, anticancer and larvicidal activities. *Plant Cell Rep*. 2020;39:921-939.
- Singh P, Mijakovic I. Strong antimicrobial activity of silver nanoparticles obtained by the green synthesis in *Viridibacillus* sp. extracts. *Front. Microbiol*. 2022;13.
- He Y, Wei F, Ma Z, Zhang H, Yang Q, Yao B, et al. Green synthesis of silver nanoparticles using seed extract of *Alpinia katsumadai*, and their antioxidant, cytotoxicity, and antibacterial activities. *RSC Adv*. 2017;7:39842-39851.
- Raj S, Trivedi R, Soni V. Biogenic synthesis of silver nanoparticles, characterization and their applications—a review. *Surfaces*. 2021;5:67-90.
- Mat Yusuf SNA, Che Mood CNA, Ahmad NH, Sandai D, Lee CK, Lim V. Optimization of biogenic synthesis of silver nanoparticles from flavonoid-rich *Clinacanthus nutans* leaf and stem aqueous extracts. *R. Soc. Open Sci*. 2020;7:200065.
- Nguyen NTT, Nguyen LM, Nguyen TTT, Nguyen TT, Nguyen DTC, Tran TV. Formation, antimicrobial activity, and biomedical performance of plant-based nanoparticles: a review. *Environ. Chem. Lett*. 2022:1-41.
- Chakravarty A, Ahmad I, Singh P, Sheikh MUD, Aalam G, Sagadevan S, et al. Green synthesis of silver nanoparticles using fruits extracts of *Syzygium cumini* and their bioactivity. *Chem. Phys. Lett*. 2022;795:139493.
- Giri AK, Jena B, Biswal B, Pradhan AK, Arakha M, Acharya S, et al. Green synthesis and characterization of silver nanoparticles using *Eugenia roxburghii* DC. extract and activity against biofilm-producing bacteria. *Sci. Rep*. 2022;12:1-9.

24. Sharifi-Rad M, Pohl P, Epifano F, Álvarez-Suarez JM. Green synthesis of silver nanoparticles using *Astragalus tribuloides* delile. root extract: Characterization, antioxidant, antibacterial, and anti-inflammatory activities. *Nanomaterials*. 2020;10:2383.
25. Rajkumar G, Sundar R. Biogenic one-step synthesis of silver nanoparticles (AgNPs) using an aqueous extract of *Persea americana* seed: Characterization, phytochemical screening, antibacterial, antifungal and antioxidant activities. *Inorg. Chem. Commun.* 2022;143:109817.
26. Olabemiwo OM, Akintelu SA, Waheed AA, Okunlola DS, Akinwale DR, Adeyinka GC, et al. Green synthesis of silver nanoparticles using stem bark extract of *Annona senegalensis*: characterization and its antibacterial potency. *Curr. Res. Green Sustain. Chem.* 2021;4:100219.
27. Imchen P, Ziekhrü M, Zhimomi BK, Phucho T. Biosynthesis of silver nanoparticles using the extract of *Alpinia galanga* rhizome and *Rhus semialata* fruit and their antibacterial activity. *Inorg. Chem. Commun.* 2022:109599.
28. Elbali W, Djouahri A, Djerrad Z, Saka B, Aberrane S, Sabaou N, et al. Chemical variability and biological activities of *Marrubium vulgare* L. essential oil, depending on geographic variation and environmental factors. *J. Essent. Oil Res.* 2018;30:470-487.
29. Boudjelal A, Henchiri C, Siracusa L, Sari M, Ruberto G. Compositional analysis and in vivo anti-diabetic activity of wild Algerian *Marrubium vulgare* L. infusion. *Fitoterapia*. 2012;83:286-292.
30. Zarai Z, Kadri A, Ben Chobba I, Ben Mansour R, Bekir A, Mejdoub H, et al. The in-vitro evaluation of antibacterial, antifungal and cytotoxic properties of *Marrubium vulgare* L. essential oil grown in Tunisia. *Lipids Health Dis.* 2011;10:1-8.
31. Miloudi K, Hamimed A, Benmimoun Y, Bellebna Y, Taibi A, Tilmatine A. Intensification of essential oil extraction of the *Marrubium vulgare* using pulsed electric field. *J. Essent. Oil-Bear.* 2018;21:811-824.
32. Benarous K, Benali FZ, Bekhaoua IC, Yousfi M. Novel potent natural peroxidases inhibitors with in vitro assays, inhibition mechanism and molecular docking of phenolic compounds and alkaloids. *J. Biomol. Struct. Dyn.* 2021;39:7168-7180.
33. Mehalaine S, Chenchouni H. New insights for the production of medicinal plant materials: Ex vitro and in vitro propagation of valuable Lamiaceae species from northern Africa. *Curr. Plant Biol.* 2021;27:100216.
34. Boulila A, Sanaa A, Salem IB, Rokbeni N, M'rabet Y, Hosni K, et al. Antioxidant properties and phenolic variation in wild populations of *Marrubium vulgare* L.(Lamiaceae). *Ind. Crops. Prod.* 2015;76:616-622.
35. Martino E, Della Volpe S, Cavalloro V, Amri B, Kaab LBB, Marrubini G, et al. The use of a microwave-assisted solvent extraction coupled with HPLC-UV/PAD to assess the quality of *Marrubium vulgare* L.(white horehound) herbal raw material. *Phytochem. Anal.* 2019;30:377-384.
36. Aćimović M, Jeremić K, Salaj N, Gavarić N, Kiprović B, Sikora V, et al. *Marrubium vulgare* L.: A phytochemical and pharmacological overview. *Molecules*. 2020;25:2898.
37. Rezgui M, Basma M, Neng N, Nogueira JM, Bettaieb Ben-Kaab L, Machado Araújo ME. Evaluation of *marrubium vulgare* growing wild in Tunisia for its potential as a dietary supplement. *Foods*. 2021;10:2864.
38. Lupuliasa AI, Prisada RM, Matei RI, Avramescu SM, Vasile BŞ, Fierascu RC, et al. Development of Biologically Active Phytosynthesized Silver Nanoparticles Using *Marrubium vulgare* L. Extracts: Applications and Cytotoxicity Studies. *Nanomaterials*. 2024;14:895.
39. Singh C, Kumar J, Kumar P, Chauhan BS, Tiwari KN, Mishra SK, et al. Green synthesis of silver nanoparticles using aqueous leaf extract of *Premna integrifolia* (L.) rich in polyphenols and evaluation of their antioxidant, antibacterial and cytotoxic activity. *Biotechnol. Biotechnol. Equip.* 2019;33:359-371.
40. Asimuddin M, Shaik MR, Adil SF, Siddiqui MRH, Alwarthan A, Jamil K, et al. *Azadirachta indica* based biosynthesis of silver nanoparticles and evaluation of their antibacterial and cytotoxic effects. *J. King Saud Univ. Sci.* 2020;32:648-656.
41. Nanda A, Saravanan M. Biosynthesis of silver nanoparticles from *Staphylococcus aureus* and its antimicrobial activity against MRSA and MRSE. *Nanomed. Nanotechnol. Biol. Med.* 2009;5:452-456.
42. Arsene MM, Viktorovna PI, Alla MV, Mariya MA, Sergei GV, Cesar E, et al. Optimization of ethanolic extraction of *Enantia chloranta* bark, phytochemical composition, green synthesis of silver nanoparticles, and antimicrobial activity. *Ferment.* 2022;8:530.
43. Mussin J, Robles-Botero V, Casañas-Pimentel R, Rojas F, Angiolella L, Martín-Martínez S, et al. Antimicrobial and cytotoxic activity of green synthesis silver nanoparticles targeting skin and soft tissue infectious agents. *Sci. Rep.* 2021;11:1-12.
44. Rizwana H, Aljowaie RM, Al Otibi F, Alwahibi MS, Alharbi SA, Al Asmari SA, et al. Antimicrobial and antioxidant potential of the silver nanoparticles synthesized using aqueous extracts of coconut meat (*Cocos nucifera* L.). *Sci. Rep.* 2023;13:16270.
45. Ghedadba N, Hambaba L, Fercha N, Houas B, Abdessemed S, Mokhtar S. Assessment of hemostatic activity of the aqueous extract of leaves of *Marrubium vulgare* L., a Mediterranean Lamiaceae Algeria. *Int. J. Health Sci.* 2016;2:253-258.
46. Namoune I, Khettal B, Assaf A, Elhayek S, Arrar L. Antioxidant and anti-inflammatory activities of organic and aqueous extracts of northeast Algerian *Marrubium vulgare*. *Phytothérapie*. 2018;16:S119-S129.
47. Al-Otibi F, Alkhudhair SK, Alharbi RI, Al-Askar AA, Aljowaie RM, Al-Shehri S. The antimicrobial activities of silver nanoparticles from aqueous extract of grape seeds against pathogenic bacteria and fungi. *Molecules*. 2021;26:6081.
48. Urnukhsaikhan E, Bold B-E, Gunbileg A, Sukhbaatar N, Mishig-Ochir T. Antibacterial activity and characteristics of silver nanoparticles biosynthesized from *Carduus crispus*. *Sci. Rep.* 2021;11:1-12.
49. Anbazhagan S, Azeez S, Morukattu G, Rajan R, Venkatesan K, Thangavelu KP. Synthesis, characterization and biological applications of mycosynthesized silver nanoparticles. *3 Biotech.* 2017;7:1-9.
50. Gupta P, Rai N, Verma A, Saikia D, Singh SP, Kumar R, et al. Green-Based Approach to Synthesize Silver Nanoparticles Using the Fungal Endophyte *Penicillium oxalicum* and Their Antimicrobial, Antioxidant, and In Vitro Anticancer Potential. *ACS omega*. 2022.
51. Sarsar V, Selwal MK, Selwal KK. Biogenic synthesis, optimisation and antibacterial efficacy of extracellular silver nanoparticles using novel fungal isolate *Aspergillus fumigatus* MA. *IET Nanobiotechnol.* 2016;10:215-221.
52. Verma DK, Hasan SH, Banik RM. Photo-catalyzed and phyto-mediated rapid green synthesis of silver nanoparticles using herbal extract of *Salvinia molesta* and its antimicrobial efficacy. *J. Photochem. Photobiol. B: Biol.* 2016;155:51-59.
53. Singh J, Dhaliwal AS. Novel green synthesis and characterization of the antioxidant activity of silver nanoparticles prepared from *Nepeta leucophylla* root extract. *Anal. Lett.* 2019;52:213-230.
54. Tamilarasi P, Meena P. Green synthesis of silver nanoparticles (Ag NPs) using *Gomphrena globosa* (Globe amaranth) leaf extract and their characterization. *Mater. Today: Proc.* 2020;33:2209-2216.
55. Ssekatawa K, Byarugaba DK, Kato CD, Wampande EM, Ejobi F, Nakavuma JL, et al. Green strategy-based synthesis of silver nanoparticles for antibacterial applications. *Front. Nanotechnol.* 2021:59.

56. Santos AP, Gonçalves MM, Justus B, Fardin DPdS, Toledo ACO, Budel JM, et al. Calendula officinalis L. flower extract-mediated green synthesis of silver nanoparticles under LED light. *Braz. J. Pharm. Sci.* 2022;58.
57. Khan M, Khan M, Adil SF, Tahir MN, Tremel W, Alkhatlan HZ, et al. Green synthesis of silver nanoparticles mediated by Pulicaria glutinosa extract. *Int. J. Nanomed.* 2013;8:1507.
58. Salehi S, Shandiz SAS, Ghanbar F, Darvish MR, Ardestani MS, Mirzaie A, et al. Phytosynthesis of silver nanoparticles using Artemisia marschalliana Sprengel aerial part extract and assessment of their antioxidant, anticancer, and antibacterial properties. *Int. J. Nanomed.* 2016;11:1835.
59. Okaiyeto K, Hoppe H, Okoh AI. Plant-based synthesis of silver nanoparticles using aqueous leaf extract of Salvia officinalis: characterization and its antiplasmodial activity. *J. Cluster Sci.* 2021;32:101-109.
60. Sithara R, Selvakumar P, Arun C, Anandan S, Sivashanmugam P. Economical synthesis of silver nanoparticles using leaf extract of Acalypha hispida and its application in the detection of Mn (II) ions. *J. Adv. Res.* 2017;8:561-568.
61. Han Z, Jiang X. Microfluidic synthesis of functional nanoparticles. *Nanotechnology and Microfluidics.* 2020:319-345.
62. Sharma P, Pant S, Rai S, Yadav RB, Sharma S, Dave V. Green synthesis and characterization of silver nanoparticles by Allium cepa L. to produce silver nano-coated fabric and their antimicrobial evaluation. *Appl. Organomet. Chem.* 2018;32:e4146.
63. Yeap SP. Permanent agglomerates in powdered nanoparticles: Formation and future prospects. *Powder Technol.* 2018;323:51-59.
64. Balashanmugam P, Kalaichelvan PT. Biosynthesis characterization of silver nanoparticles using Cassia roxburghii DC. aqueous extract, and coated on cotton cloth for effective antibacterial activity. *Int. J. Nanomed.* 2015;10:87.
65. Ali K, Ahmed B, Dwivedi S, Saquib Q, Al-Khedhairi AA, Musarrat J. Microwave accelerated green synthesis of stable silver nanoparticles with Eucalyptus globulus leaf extract and their antibacterial and antibiofilm activity on clinical isolates. *PLoS ONE.* 2015;10:e0131178.
66. Skandalis N, Dimopoulou A, Georgopoulou A, Gallios N, Papadopoulos D, Tsipas D, et al. The effect of silver nanoparticles size, produced using plant extract from Arbutus unedo, on their antibacterial efficacy. *Nanomaterials.* 2017;7:178.
67. He Y, Du Z, Ma S, Cheng S, Jiang S, Liu Y, et al. Biosynthesis, antibacterial activity and anticancer effects against prostate cancer (PC-3) cells of silver nanoparticles using Dimocarpus Longan Lour. peel extract. *Nanoscale Res. Lett.* 2016;11:1-10.
68. Ojo OA, Oyinloye BE, Ojo AB, Ajiboye BO, Olayide II, Idowu O, et al. Green-route mediated synthesis of silver nanoparticles (AgNPs) from syzygium cumini (L.) Skeels polyphenolic-rich leaf extracts and investigation of their antimicrobial activity. *IET Nanobiotechnol.* 2018;12:305-310.
69. Soares MR, Corrêa RO, Stroppa PHF, Marques FC, Andrade GF, Correa CC, et al. Biosynthesis of silver nanoparticles using Caesalpinia ferrea (Tul.) Martius extract: physicochemical characterization, antifungal activity and cytotoxicity. *PeerJ.* 2018;6:e4361.
70. Malathi S, Manikandan D, Nishanthi R, Jagan EG, Riyaz SUM, Palani P, et al. Silver Nanoparticles, Synthesized using Hyptis suaveolens (L) Poit and their Antifungal Activity against Candida spp. *ChemistrySelect.* 2022;7:e202203050.
71. Garibo D, Borbón-Nuñez HA, de León JND, García Mendoza E, Estrada I, Toledano-Magaña Y, et al. Green synthesis of silver nanoparticles using Lysiloma acapulcensis exhibit high-antimicrobial activity. *Sci. Rep.* 2020;10:1-11.
72. Ansari MA, Alzohairy MA. One-pot facile green synthesis of silver nanoparticles using seed extract of Phoenix dactylifera and their bactericidal potential against MRSA. *Evid. Based Complement. Alternat. Med.* 2018;2018.
73. Qayyum S, Oves M, Khan AU. Obliteration of bacterial growth and biofilm through ROS generation by facilely synthesized green silver nanoparticles. *PLoS ONE.* 2017;12:e0181363.
74. Agnihotri S, Mukherji S, Mukherji S. Size-controlled silver nanoparticles synthesized over the range 5–100 nm using the same protocol and their antibacterial efficacy. *RSC Adv.* 2014;4:3974-3983.
75. Cheon JY, Kim SJ, Rhee YH, Kwon OH, Park WH. Shape-dependent antimicrobial activities of silver nanoparticles. *Int. J. Nanomed.* 2019:2773-2780.
76. Raza MA, Kanwal Z, Rauf A, Sabri AN, Riaz S, Naseem S. Size- and shape-dependent antibacterial studies of silver nanoparticles synthesized by wet chemical routes. *Nanomaterials.* 2016;6:74.
77. Bedlovicová Z, Salayová A. Green-synthesized silver nanoparticles and their potential for antibacterial applications. *Bacterial Pathogenesis and Antibacterial Control.* 2017.
78. Dong Y, Zhu H, Shen Y, Zhang W, Zhang L. Antibacterial activity of silver nanoparticles of different particle size against Vibrio Natriegens. *PLoS ONE.* 2019;14:e0222322.
79. Salleh A, Naomi R, Utami ND, Mohammad AW, Mahmoudi E, Mustafa N, et al. The potential of silver nanoparticles for antiviral and antibacterial applications: A mechanism of action. *Nanomaterials.* 2020;10:1566.
80. Dubey D, Meher RK, Pradhan B, Induar S, Kar B, Naik PK, et al. Green synthesis of silver nanoparticles using leaf extract of Woodfordia fruticosa (L.) for potential therapeutic application. *J. Chem. Technol. Biotechnol.*
81. Srečković NZ, Nedić ZP, Monti DM, D'Elia L, Dimitrijević SB, Mihailović NR, et al. Biosynthesis of silver nanoparticles using Salvia pratensis L. aerial part and root extracts: Bioactivity, biocompatibility, and catalytic potential. *Molecules.* 2023;28:1387.
82. Alfaro S, Acuña V, Ceriani R, Cavieres MF, Weinstein-Oppenheimer CR, Campos-Estrada C. Involvement of inflammation and its resolution in disease and therapeutics. *Int. J. Mol. Sci.* 2022;23:10719.
83. Doran AC. Inflammation resolution: implications for atherosclerosis. *Circ. Res.* 2022;130:130-148.
84. Yattoo MI, Gopalakrishnan A, Saxena A, Parray OR, Tufani NA, Chakraborty S, et al. Anti-inflammatory drugs and herbs with special emphasis on herbal medicines for countering inflammatory diseases and disorders-a review. *Recent patents on inflammation & allergy drug discovery.* 2018;12:39-58.
85. Silvestrini B, Silvestrini M. Medical implications of the relationships among protein denaturation, necrosis and inflammation: an intriguing story. *Tendons-Trauma, Inflammation, Degeneration, and Treatment.* IntechOpen; 2022.
86. Aitbaba A, Kabdy H, Fatimzahra A, Azraida H, Abdoussadeq O, Aboufatima R, et al. Anti-inflammatory and antiarthritic properties of Marrubium vulgare aqueous extract in an animal model. *Nat. Prod. Res.* 2024:1-9.
87. Dasgupta N, Ranjan S, Patra D, Srivastava P, Kumar A, Ramalingam C. Bovine serum albumin interacts with silver nanoparticles with a "side-on" or "end on" conformation. *Chem. Biol. Interact.* 2016;253:100-111.

GRAPHICAL ABSTRACT



Cite this article: Abbad S, Aissaoui N, Gana FZ. *Marrubium vulgare* Leaf Extract-Assisted Green Synthesis of Silver Nanoparticles: Optimization, Characterization and In Vitro Exploration of Their Antimicrobial, Antioxidant and Anti-Inflammatory Potential. *Pharmacogn J.* 2025;17(1): 7-21.